Check for updates

2-Acyl-1,1,3,3-tetracyanopropenides (ATCN): structure characterization and luminescence properties of ammonia and alkali metal ATCN salts†

Ya. S. Kayukov,[a] S. V. Karpov, ID *[a] A. A. Grigor'ev,[a] O. E. Nasakin,[a] V. A. Tafeenko,[b] K. A. Lyssenko, ID [c] A. V. Shapovalov[c] and E. A. Varaksina[d]

Herein, syntheses, crystal structures, and photoluminescence properties of 24 new ammonia and alkali metal ATCN salts characterized *via* single-crystal X-ray diffraction are reported. Moreover, ten structure types of these salts have been described, three of which are predominant. Some ATCNs were obtained as two crystal-line polymorphs. It was estimated that most ATCN powders exhibited yellow-green fluorescence (at 450–600 nm). For samples that possess fluorescence of low intensity in the solid state, several optical centers of emission exist. It was speculated that the obtained spectral features were due to anion-anion inter-molecular interactions. ATCN being a new representative of stable tetracyanoallyl salts is a promising candi-date for creation of various 1D, 2D, and 3D supramolecular structures and potential functional materials.

Introduction

The coordination chemistry of salts[1] and coordination poly-mers[2] containing tetracyanoallyl (TCA) anion has been inten-sively studied because of the diverse nature of applications and potentially useful properties, such as semiconducting,[3] thermo- and photochromic,[4] magnetic,[5] and photomagnetic properties,[6] of these materials. TCA ligands have also received interest for creation of spin-crossover (SCO) materials,[7] ionic liquids,[8] (including radiolysis resistant IL,[9] efficient propel-lants,[10] and burning-rate (BR) catalysts).[11] Moreover, in recent studies, TCA ligands have found application as components of redox electrocatalysts[12] and fluorine-free solid-polymer electro-lytes for sodium-ion batteries.[13] Some TCA complexes have also shown antimicrobial activity.[14]

In this study, we continued the systematic study of new representatives of TCA salts, 2-acyl-1,1,3,3-tetracyanoprope-nides (ATCN). These salts are stable and can be easily obtained from readily available reagents.[15] For the obtained salts, the absorption and fluorescence spectra both in the solution and solid state were acquired. The obtained spectral data were com-pared with the results of X-ray experiments to find out the cor-relations between ammonia and alkali metal ATCN structure and their fluorescence properties.

Among a broad range of TCA ligands, ATCN are noteworthy because they contain an acyl group at position 2 of TCA anion, and the carbonyl oxygen can form an additional coordination bond with the cation (Fig. 1).
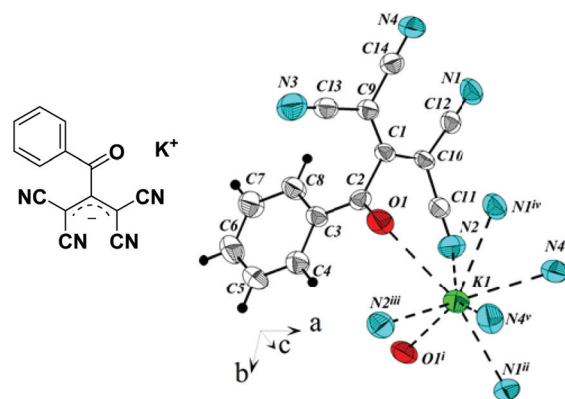
[a]*I. N. Ul'yanov Chuvash State University, Moskovskii Prospekt 15, Cheboksary, 428015, Russia. E-mail: serg31.chem@mail.ru*
[b]*Lomonosov Moscow State University, Leninskiye Gory 1-3, Moscow, 119991, Russia*
[c]*A. N. Nesmeyanov Institute of Organoelement Compounds, Russian Academy of Sciences (INEOS RAS), 119991 Moscow, Russia*
[d]*P.N. Lebedev Physical Institute of the Russian Academy of Sciences (FIAN), 119991 Moscow, Russia*

Fig. 1 Potassium 2-benzoyl-1,1,3,3-tetracyanopropenide **β-1d**. Coordination environment of K with 50% probability ellipsoids. Bond distances are 3.035 (K1···O1), 3.020 (K1···N1), 2.801 (K1···O1^i), 2.862 (K1···N1^{ii}), 2.844 (K1···N2^{iii}), 2.978 (K1···N1^{iv}), 3.137 (K1···N4^{iv}), and 2.944 (K1···N4^v) Å.

Some ATCNs were obtained as two crystalline polymorphs. In this case, we designated them as α and β. The conditions for their formation are different. α-Forms were obtained by slow evaporation of the solvent at r.t., whereas β-forms were isolated *via* rapid evaporation of a warm solution.

The ORTEP images, additional crystallographic data, and methods of single crystal preparation are presented in the ESI.†

Designation of ATCN salts

Anion	Cation	Label	Name
(2-benzoyl-1,1,3,3-tetracyanopropenide)	NH_4^+	**1a**	Ammonium 2-benzoyl-1,1,3,3-tetracyanopropenide
	Li^+	**1b**	Lithium 2-benzoyl-1,1,3,3-tetracyanopropenide
	Na^+	**1c**	Sodium 2-benzoyl-1,1,3,3-tetracyanopropenide
	K^+	**1d**	Potassium 2-benzoyl-1,1,3,3-tetracyanopropenide
	Rb^+	**1e**	Rubidium 2-benzoyl-1,1,3,3-tetracyanopropenide
	Cs^+	**1f**	Cesium 2-benzoyl-1,1,3,3-tetracyanopropenide
(2-(4′-methylbenzoyl)-1,1,3,3-tetracyanopropenide)	NH_4^+	**2a**	Ammonium 2-(4′-methylbenzoyl)-1,1,3,3-tetracyanopropenide
	Li^+	**2b**	Lithium 2-(4′-methylbenzoyl)-1,1,3,3-tetracyanopropenide
	Na^+	**2c**	Sodium 2-(4′-methylbenzoyl)-1,1,3,3-tetracyanopropenide
	K^+	**2d**	Potassium 2-(4′-methylbenzoyl)-1,1,3,3-tetracyanopropenide
	Rb^+	**2e**	Rubidium 2-(4′-methylbenzoyl)-1,1,3,3-tetracyanopropenide
	Cs^+	**2f**	Cesium 2-(4′-methylbenzoyl)-1,1,3,3-tetracyanopropenide
(2-(4′-methoxybenzoyl)-1,1,3,3-tetracyanopropenide)	NH_4^+	**3a**	Ammonium 2-(4′-methoxybenzoyl)-1,1,3,3-tetracyanopropenide
	Li^+	**3b**	Lithium 2-(4′-methoxybenzoyl)-1,1,3,3-tetracyanopropenide
	Na^+	**3c**	Sodium 2-(4′-methoxybenzoyl)-1,1,3,3-tetracyanopropenide
	K^+	**3d**	Potassium 2-(4′-methoxybenzoyl)-1,1,3,3-tetracyanopropenide
	Rb^+	**3e**	Rubidium 2-(4′-methoxybenzoyl)-1,1,3,3-tetracyanopropenide
	Cs^+	**3f**	Cesium 2-(4′-methoxybenzoyl)-1,1,3,3-tetracyanopropenide
(2-(4′-bromobenzoyl)-1,1,3,3-tetracyanopropenide)	NH_4^+	**4a**	Ammonium 2-(4′-bromobenzoyl)-1,1,3,3-tetracyanopropenide
	Li^+	**4b**	Lithium 2-(4′-bromobenzoyl)-1,1,3,3-tetracyanopropenide
	Na^+	**4c**	Sodium 2-(4′-bromobenzoyl)-1,1,3,3-tetracyanopropenide
	K^+	**4d**	Potassium 2-(4′-bromobenzoyl)-1,1,3,3-tetracyanopropenide
	Rb^+	**4e**	Rubidium 2-(4′-bromobenzoyl)-1,1,3,3-tetracyanopropenide
	Cs^+	**4f**	Cesium 2-(4′-bromobenzoyl)-1,1,3,3-tetracyanopropenide

Results and discussion

Description of ATCN crystal packing

Type 1. This type of crystal packing was found in compounds **1a**, **4a**, and **4e**. The crystals are triclinic, and the space group is $P\bar{1}$. In this case, ATCN anions are lined up in chains in a head-to-tail arrangement along one of the crystallographic axes. Every two neighboring chains are connected by a center of symmetry. Each cation coordinates five anions from four neighboring chains (Fig. 2). Fig. 3 shows the resulting formation of the 3D ionic structure of these salts.

Contrary to the crystal **1a**, in the independent part of the unit cell of the crystals **4a** and **4e**, there are two crystallographically independent types of ATCN anions (designated as blue and red in Fig. 4b). These anions form layers in the *b*–*a* plane that alternate with each other.

Type 2. This type of crystal packing was found in the compounds **β-1c**, **β-1d**, **3c**, **3a**, and **α-3d**. The crystals are monoclinic, and the space group is $P2_1/c$. In this case, ATCN anions are lined up in rows in a head-to-tail arrangement along one of the crystallographic axes. Moreover, two adjacent rows are wedged into each other by aryl rings like the fingers in a lock. The result is a stack having the topology of a half-cylinder or gutter. The three gutters form a channel inside, which is a chain of cations (Fig. 5). Fig. 6 shows the general crystal packing.

Sodium 2-benzoyl-1,1,3,3-tetracyanopropenide **β-1c** has a layered 2D ion-molecular structure, as shown in Fig. 6. Each layer was formed by sodium chains, which were united by water bridges and ATCN anions. Each sodium cation coordinates four ATCN anions (Fig. 7). The salt **3c** has an analogous structure.

The salts **3a**, **β-1d**, and **α-3d** do not contain crystallization water. Each cation coordinates six ATCN anions, and the cations are linked in chains *via* nitrogen bridges (Fig. 8).

Fig. 9 shows the general crystal packing of **β-1d**. The salts **3a** and **α-3d** have an analogous structure.

Type 3. This type of crystal packing was found in the compounds **2d**, **4d**, **2e**, **2f**, **β-3d**, and **3e**. The crystals of **2d**, **4d**, **2e**,
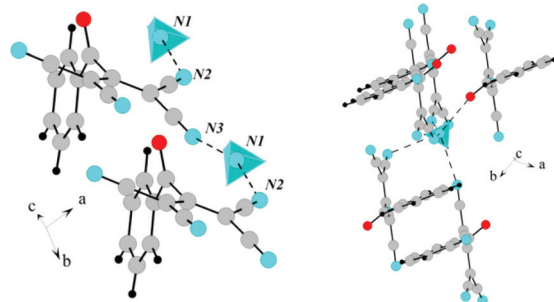

Fig. 2 The arrangement of ATCN anions in the crystal of **1a**. Gray, red, and blue spheres represent carbon, oxygen, and nitrogen atoms, respectively. Blue tetrahedra are ammonia cations.
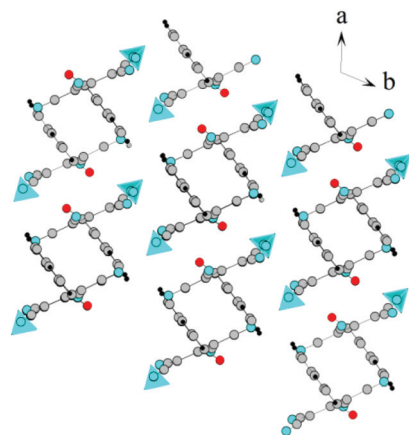
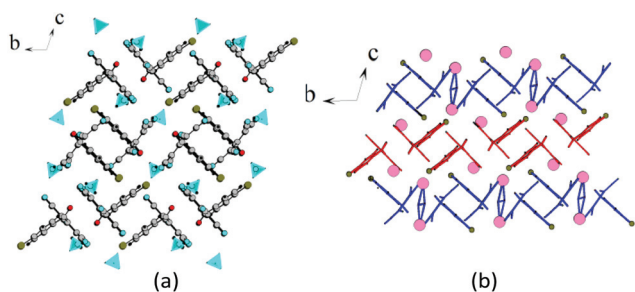**Fig. 3** Fragment of the crystal lattice of **1a** viewed along the *c* axis.

Fig. 4 Fragment of the crystal lattice of **4a** (a) and **4e** (b) viewed along the *c* axis. Olive and pink spheres represent bromine and rubidium atoms, respectively.
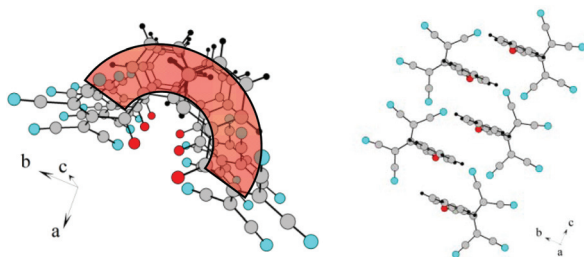

Fig. 5 Schematic of packing in the stacks of ATCN anions in **β-1c**. The sodium cations are hidden.

Fig. 6 (a) Fragment of the crystal lattice of **β-1c** viewed along the *c* axis. Magenta spheres represent sodium atoms. (b) General schematic of the crystal packing.
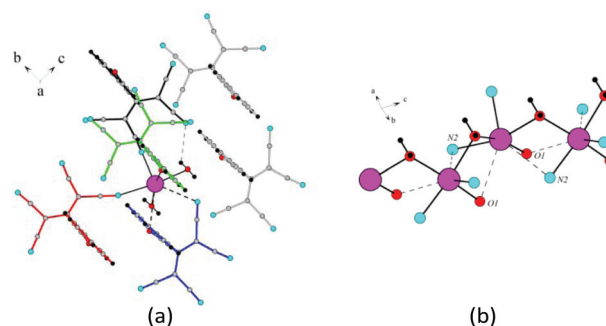
Fig. 7 (a) Coordination environment of Na in **β-1c**. (b) Sodium cations united by water bridges. Na···Na distances are 3.779 Å.
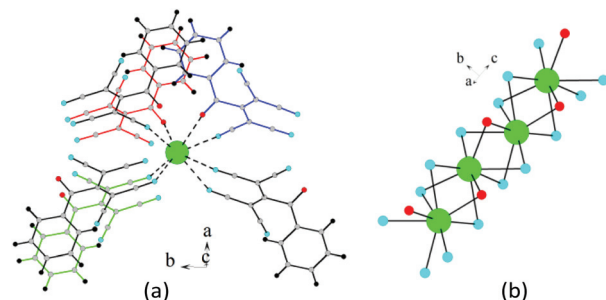

Fig. 8 (a) Coordination environment of K (green sphere) in **β-1d**. (b) Potassium cations united by nitrogen bridges. K···K distances are 3.618 Å.

and **2f** are monoclinic, and the space group is *P*21/*c*. The crystals of **β-3d** and **3e** are triclinic, and the space group is *P*1̄.

In the crystal of **2d**, each potassium cation coordinates five ATCN anions belonging to three neighboring gutters. The cations are linked in chains *via* oxygen O1 and nitrogen N4 bridges (K···K distance is 4.705 Å). The chains are packed in 2D sheets *via* N3 nitrogens (K···K distance is 4.438 Å), as shown in Fig. 10.

Fig. 11 shows the general crystal packing of **2d**. The salts **4d**, **2e**, and **2f** have an analogous structure.

The salts **β-3d** and **3e** have an analogous structure with a minor difference. The crystal lattice of **β-3d** is composed of two types of crystallographically independent ATCN anions.

They alternate in gutters, and the methoxy groups are disordered. The alternating ions K1 and K2 are also connected *via* bridging heteroatoms belonging to ATCN anions; this results in the formation of the 2D sheet in the *a*–*b* plane (Fig. 12(a)). The distances between potassium cations alternate (the distance between K1···K2 that is bonded *via* O1A and N4 is 4.596 Å, whereas the distance between K1···K2 that is bonded *via* O1 and N1A is 4.654 Å). The bridging nitrogen N2A connects K2 cations (K2···K2 distance is 4.445 Å). The nitrogen N3 connects the K1 cations (K1···K1 distance is 4.451 Å). For the rest, the architecture of the crystals is the same as in **2d** (Fig. 12(b)). The salt **3e** has an analogous structure.
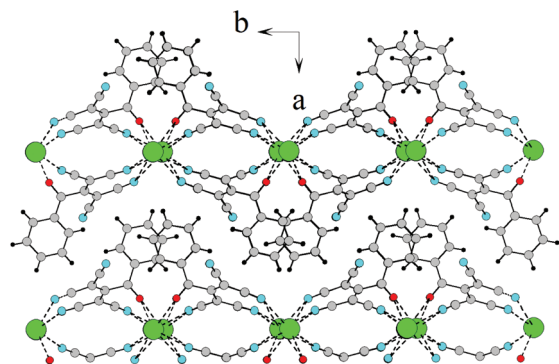
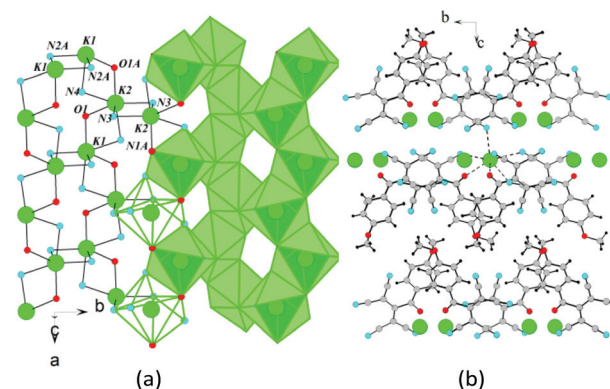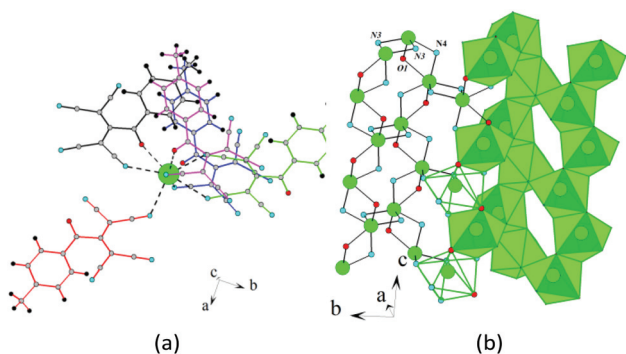**Fig. 9** Fragment of the crystal lattice of β-1d viewed along the c axis.

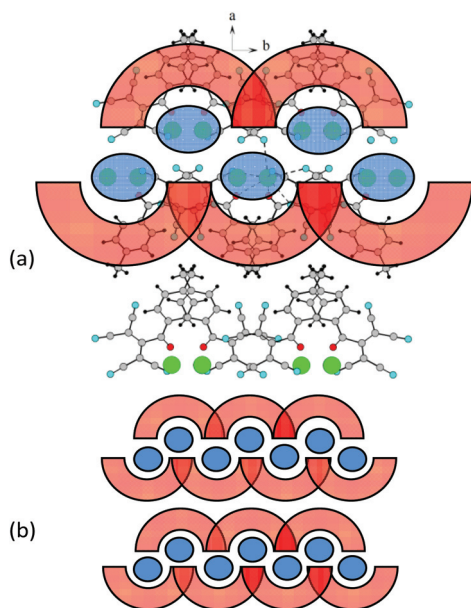**Fig. 10** (a) Coordination environment of K in 2d. (b) Schematic of the formation of the 2D sheet in 2d.

Fig. 11 (a) Fragment of the crystal lattice of 2d viewed along the c axis. (b) General schematic of the crystal packing.
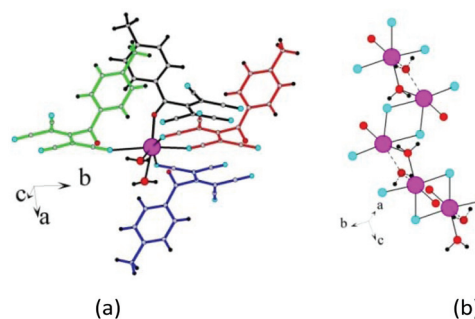

Fig. 12 (a) Schematic of the formation of the 2D sheet in β-3d. (b) Fragment of the crystal lattice of β-3d viewed along the a axis.

Type 4. This type of crystal packing was found in compounds **2a** and **β-2c**. These salts crystallize in monoclinic symmetry with the space group $C2/c$. In the crystal of **β-2c**, each sodium cation coordinates one water and four ATCN anions, belonging to three neighboring gutters. Sodium cations are united in chains via alternating nitrogen and water bridges (Fig. 13). The distance between sodium cations, which are bonded by water, is 3.890 Å, and that between those bonded by nitrogens is −3.955 Å. Fig. 14 shows the general crystal packing.

The salt **2a** has a similar crystal packing. In this case, the crystal lattice is composed of two types of crystallographically independent ATCN anions. The cations are linked to chains via bridging N1 and aqua bridges (Fig. 15).

Types 5 and 6. These types of crystal packing are characteristic for lithium ATCN **1b** (type 5) and **2b–4b** (type 6). The salt **1b** crystallizes in triclinic symmetry with the space group $P\bar{1}$. The crystals of **2b**, **3b**, and **4b** are monoclinic with the space group of $P2_1/c$.

Each lithium cation coordinates the nitrogens N1 and N2 belonging to different ATCN anions and connects them to an infinite chain. These chains are combined in pairs by coordi-
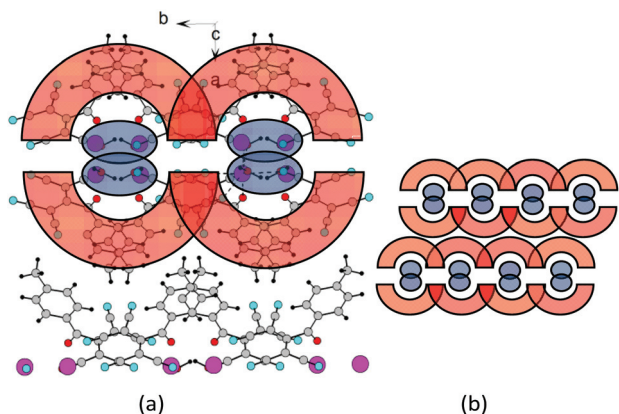

Fig. 13 (a) Coordination environment of Na in β-2c. There are two water molecules in the figure, but there is only one molecule in the crystal, which is located in one of the two indicated coordination sites with a 50% chance. (b) Sodium cations united by water and nitrogen bridges.

Fig. 14 (a) Fragment of the crystal lattice of **β-2c** viewed along the *c* axis. (b) General schematic of the crystal packing.
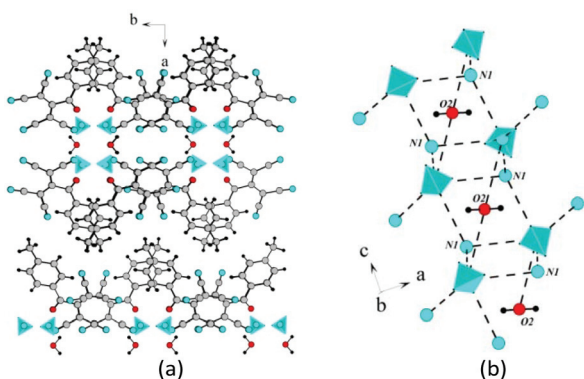

Fig. 15 (a) Fragment of the crystal lattice of **2a** viewed along the *a* axis. (b) Ammonia cations united by water and nitrogen bridges.

nation of lithium with the carbonyl oxygen; this forms a 1D chain structure. The fourth coordination site of lithium is occupied by a water molecule.

Type five: two chains are centrosymmetric (running toward each other, as shown in Fig. 16).[15a] Type six: two chains are arranged in one direction (Fig. 17).
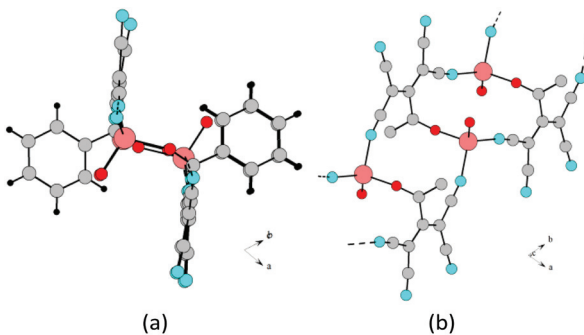
Fig. 16 (a) Fragment of the 1D chain structure of **1b** viewed along the *c* axis. (b) Schematic of the formation of 1D chain in **1b**.
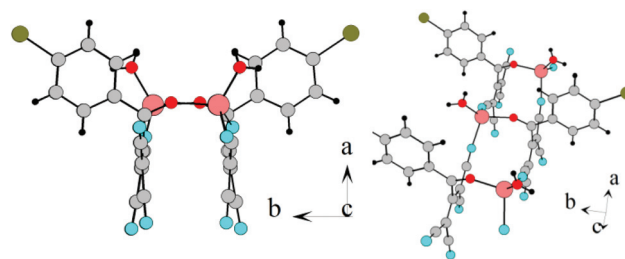
Fig. 17 (a) Fragment of the 1D chain structure of **4b** viewed along the *c* axis. (b) Schematic of the formation of 1D chain in **4b**.
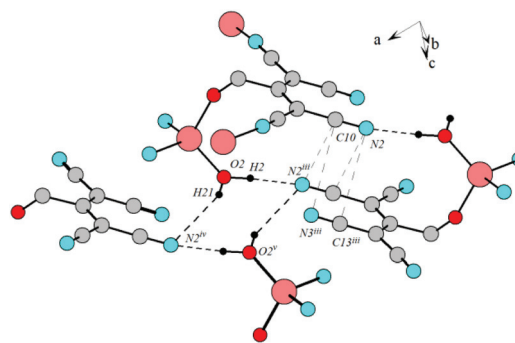
Fig. 18 Fragment of the crystal lattice of **2b**. Bond distances are O2H2⋯N2^{iii} 2.849, O2H21⋯N2^{iv} 3.320, C10⋯N3^{iii} 3.573, C10⋯N2^{iii} 3.667, and C13^{iii}⋯N2 3.563 Å.

In both cases, the hydrogen bonds between the coordination water and the nitrogen atoms of the nitrile groups as well as CN–CN dipole–dipole interactions are present in the crystal (Fig. 18).

Type 7. This type of crystal packing was found in the salts **α-2c** and **4c**. The crystals are monoclinic with the space group of *P*21/*c*. Similar to the types 2, 3, and 4, the crystals of type 7 have a layered structure. Each layer is a 2D coordination polymer, built from chains of sodium cations, combined by aqua and ATCN anions, as shown in Fig. 19(a). Each layer consists of two half-layers of ATCN anions that are arranged by the head–tail principle along the two axes *a* and *c*. Each sodium cation coordinates four anions: three from one half-layer and one from the other (Fig. 19(b)). Along the *c* axis, the cations are connected in chains *via* aqua bridges and the bridging nitrogen N1. In a crystal, the individual layers are centrosymmetrically disposed relative to one another (Fig. 20).

The salt **4c** has an analogous structure.

Type 8. This type of crystal packing was found in the salts **α-1c** and **α-1d**. The crystals are monoclinic with the space group of *P*21/*n*. In the crystal of **α-1c**, sodium cations are combined in pairs *via* two water molecules. Each ATCN anion binds to other three adjacent pairs of sodium cations, as shown in Fig. 21(a). With one anion, the bond is formed through coordination with N3 (2.493 Å); with the second
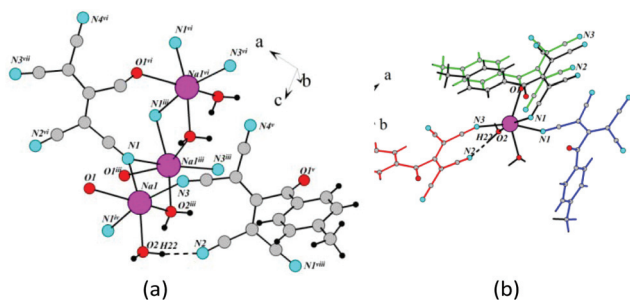
Fig. 19 (a) Sodium cations bonded by water and nitrogen bridges in **α-2c**. Na–Na distance is 3.737 Å. (b) Coordination environment of Na in **α-2c**.
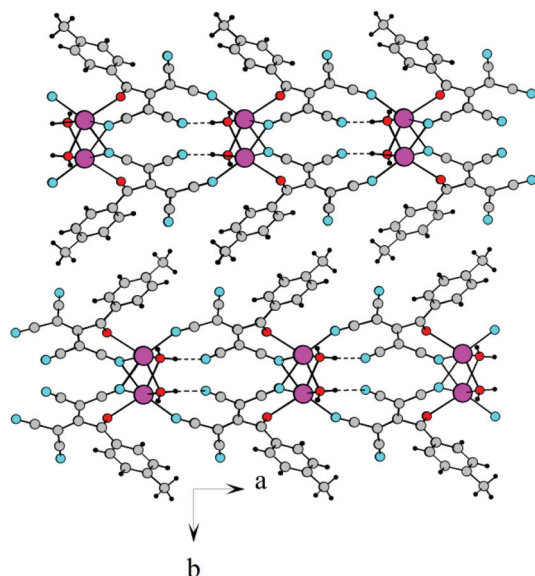

Fig. 20 2D layered structure of **α-2c**, viewed along the *c* axis.

Fig. 21 (a) Coordination environment of ATCN anion in **α-1c**. (b) 2D sheet in **α-1c**, viewed along the *a* axis.

anion, the bond is formed through carbonyl oxygen and N2 (2.452 Å), whereas with the third anion, the bond is formed *via* coordination with N1 (2.607 Å) and the hydrogen bond O2···N4 (3.011 Å). This results in the formation of a 2D sheet (Fig. 21(b)). The crystal has a layered structure.

Type 9. This type of crystal packing was found in the salts **1e** and **1f**.[15a] The crystals are monoclinic with the space group of $P2_1/c$. In the crystal of **1f**, each cesium atom coordinates five ATCN anions. Moreover, two of them (one bonded with cesium atom *via* N3, and the other bonded through N4) participate in the CN–CN dipole–dipole interaction. The tetracyanoallyl fragments of both anions are almost planar. The phenyl radical of ATCN anion bound to cesium through nitrogen N3 occupies one of the coordination sites of cesium, and the shortest contacts with C4 and C5 are 3.882 and 3.821 Å, respectively, as shown in Fig. 22(a). The third anion is bonded to cesium by two bonds through N1 and N4; thus, the N4 atom is a bridge between two cesium cations. The two other anions bonded with cesium through the carbonyl oxygen and nitrile

N2 are also in close contact with each other (the shortest C13–N1 distance is less than 3.5 Å), as shown in Fig. 22(b). Fig. 23 shows the general crystal packing.

Type 10. This type of crystal packing was found in the salt **4f**. The crystals are monoclinic with the space group of $P2_1/c$. The ATCN anions linked by cesium cations are arranged according to the head–tail principle along the *a* axis to form a chain. These chains are also arranged according to the head–tail principle along the *c* axis; this forms layers in the *a*–*c* plane. While forming a crystal, these layers are stacked centrosymmetrically relative to each other (Fig. 24).

The X-ray data was obtained using the STOE diffractometer, Pilatus 100 K detector, focusing mirror collimation, and Cu Kα (1.54086 Å) radiation in the rotation method mode. The STOE X-AREA software was used for cell refinement and data reduction. Intensity data were scaled with LANA (part of X-Area) to minimize the differences in the intensities of symmetry-equivalent reflections (multi-scan method). The structures were solved and refined with the SHELX program. The non-hydrogen atoms were refined using the anisotropic full matrix least-square procedure. Molecular geometry calculations were performed with the SHELX program, and the molecular graphics were prepared using the Diamond software.
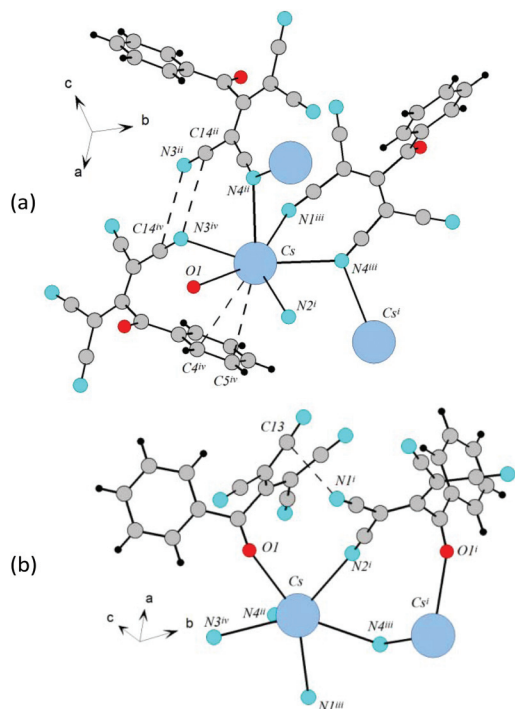
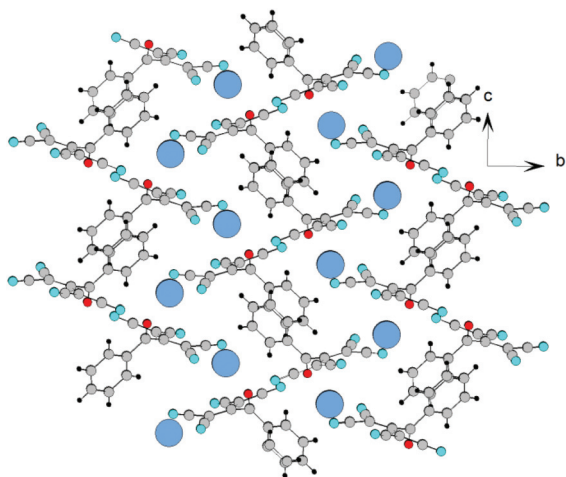**Fig. 22** Coordination environment of Cs (blue spheres) in **1f**.

Fig. 23 Fragment of the crystal lattice of **1f** viewed along the *a* axis.
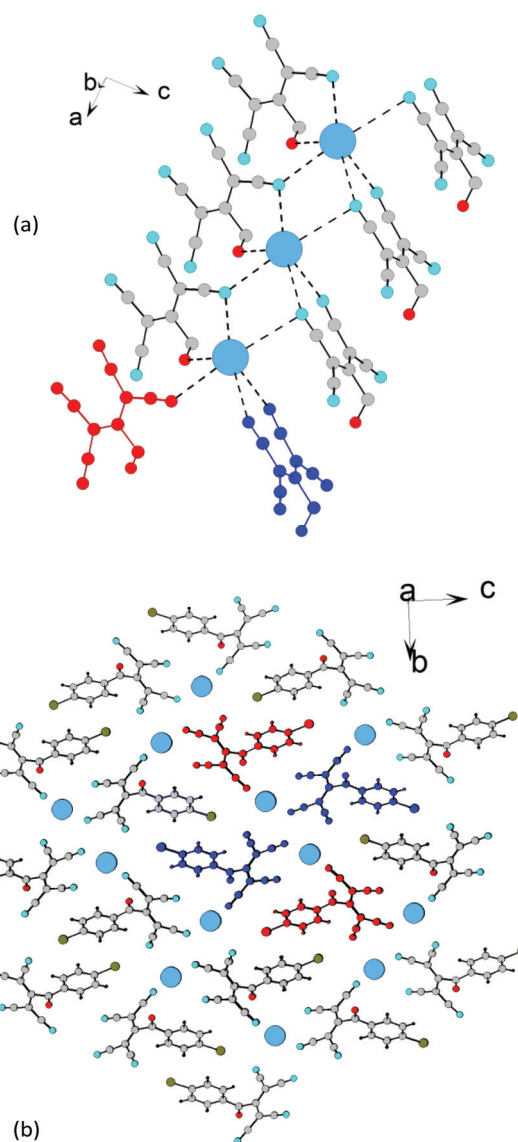

Fig. 24 (a) Schematic of the formation of 1D chains in **4f** (benzene rings are hidden). (b) Fragment of the crystal lattice of **4f** viewed along the *a* axis.

Absorption and fluorescence properties

Absorption spectra of the solutions were obtained using a Varian Cary 100 Scan spectrophotometer in a 0.1 cm layer at a concentration of 10^{-4} M in non-deaerated ethanol.

Fluorescence emission and excitation spectra of ethanol solutions and powders were obtained using a Horiba Jobin Yvon Fluorolog 3-221 fluorescence spectrometer at room temperature in a 0.1 or 0.02 cm cuvette in the reflectance mode at an angle of 7–10° for an optical density of $D \sim 0.2$ (for solutions) at the excitation wavelength.

Relative fluorescence quantum yield (φ_{rel}) of solutions was measured *vs.* a solution of 9,10-diphenylanthracene in ethanol (for non-deaerated solutions, φ = 90%),[16] and φ_{rel} accuracy was ±5% (for three measurements).

Absolute fluorescence quantum yield (φ_{abs}) of powders was measured *via* an integrating sphere G8 GMPSA with Spectralone layer,[17] and φ_{abs} accuracy was ±10% (for three measurements).

Fluorescence lifetimes (τ) were measured in the photo-counting mode with a diode laser at 369 nm and pulse length of <100 ns as the excitation source, and τ accuracy was ±10% (for three measurements).

Electronic excitation energies were calculated *via* the time-dependent density-functional theory (TD-DFT) using the Orca program package.[18]
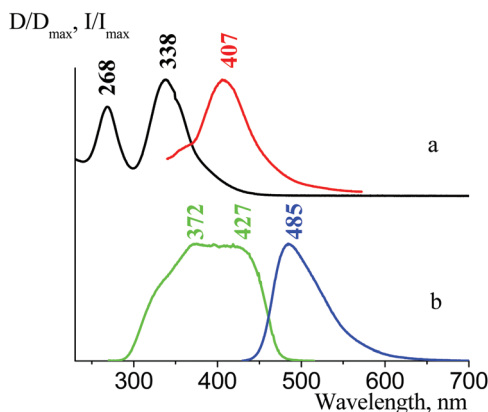
Fig. 25 (a) **2f** absorbance and emission spectra in ethanol. (b) Excitation and emission spectra in the solid state. Excitation wavelength is 320 nm (a) and 420 nm (b), and the registration wavelength is 525 nm (b).

The powders of ATCN for absorbance and fluorescence investigation were prepared from single crystals.

Absorption properties

Fig. 25(a) shows the **2f** absorbance spectrum in a dilute ethanol solution ($C \sim 10^{-4}$ mol l^{-1}). There are two bands in the absorbance spectrum with a maxima at 338 nm (ε = 45 360 L cm^{-1} mol^{-1}) and 268 nm (ε = 35 150 L cm^{-1} mol^{-1}). The absorbance spectrum of **1f** in ethanol (Fig. 26(a)) as well as those for **3f** and **4f** (see Fig. 1 and 2 in the ESI†) are almost the same. This fact led us speculate that the π-system structure of the tetracyanopropenide fragment of the ligand did not change significantly *via* the introduction of a substituent group (Br, Me, and OMe) in the *para*-position of the ligand benzene ring. The absorption spectra of salts with different cations (**2a**, **2b**, **2c**, **2d**, and **2e**) in an ethanol solution are also similar (see Fig. 3–8 in ESI†). Thus, we can conclude that the absorbance spectra of ATCNs in solution are mainly determined by electron transitions in the π-system of the tetracyanopropenide fragment of the ligand. These data are in good agreement with the results of quantum-chemical calculations (see Table 1).

Fig. 25(b) demonstrates that the **2f** solid state absorption spectrum differs from the solution spectrum: it is shifted towards longer wavelengths by about 10–20 nm and has one more band, which can only be seen as a shoulder at 380–420 nm. The **1f** solid state absorption spectrum (Fig. 26(b)) is also bathochromically shifted as compared to the solution spectrum and also has one more absorbance band in the area 400–450 nm. This indicates that in the solid state, there are intermolecular interactions, which are similar for different salts. However, the fluorescence properties of **1f** and **2f** are essentially different (see below); thus, we should find out the reason of this fact by analyzing their emission and excitation spectra.[19]
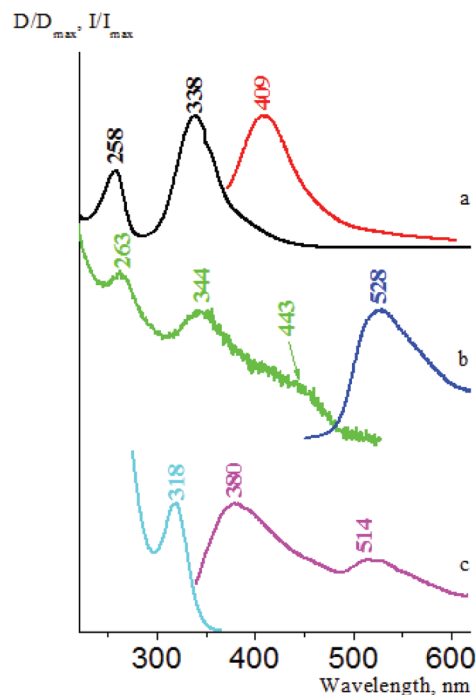

Fig. 26 **1f** absorbance (a and b), emission (a, b, and c), and excitation (c) spectra in ethanol (a) and in the solid state (b and c); excitation wavelength is 320 nm (red and magenta curves) and 420 nm (blue curve), and the registration wavelength is 380 nm (cyan curve).

Table 1 TD-DFT *ab initio* calculations for **2f** anion (isolated molecule) *via* the B3LYP method and def2-TZVPP basis and experimental values for **2f** ethanol solution

Parameter	Calculation	Experimental
λ_{max}^{abs}, nm		
S$_0$ → S$_1$	473.1	
S$_0$ → S$_2$	334.0	338
S$_0$ → S$_3$	323.3	
S$_0$ → S$_4$	299.9	
S$_0$ → S$_5$	292.1	
S$_0$ → S$_6$	279.3	
S$_0$ → S$_7$	260.2	268
S$_0$ → S$_8$	255.4	
λ_{max}^{em}, nm		
S$_1$ → S$_0$	758.2	
S$_2$ → S$_0$	398.3	407
$E_{HOMO–LUMO}$, eV		
0–0 transition	3.87	3.36[a]

[a] Determined *via* the intersection point of **2f** emission and long-wavelength absorbance bands in ethanol.

Fluorescence properties

All the investigated ATCNs possess no visible fluorescence in solution. As an example, Fig. 25(a) shows the **2f** fluorescence spectrum in ethanol, which mirrors symmetrically its long-wavelength absorption band. The relative fluorescence quantum yield φ_{rel} of **2f** ethanol solution is equal to 0.4%, and its fluorescence lifetime τ is 8.1 ns. The **1f** fluorescence spectrum in ethanol (Fig. 26(a)) is similar to that of **2f**. However, in

Table 2 Fluorescence excitation and emission maxima for the compounds **1a–4f** in the solid state (corresponding registration and excitation wavelengths are given in brackets). Images of ATCN under UV (450 nm)/visible light, and CCDC deposit numbers are also provided
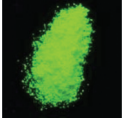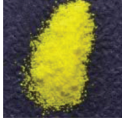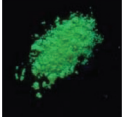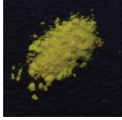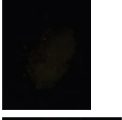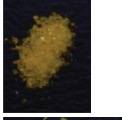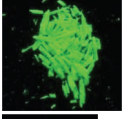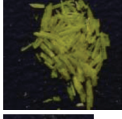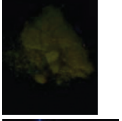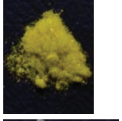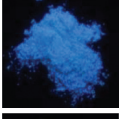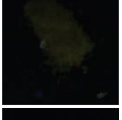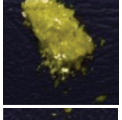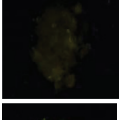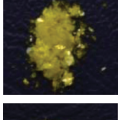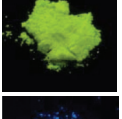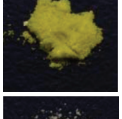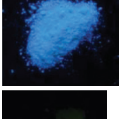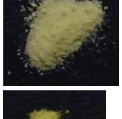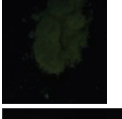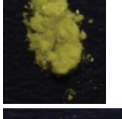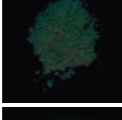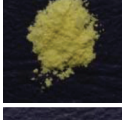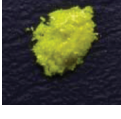
ATCN	λ_{max}^{ex} (λ^{reg}), nm	λ_{max}^{em} (λ^{ex}), nm	Visual appearance of the compounds under UV/visible light	CCDC	Structure type
1a	328~ [a], **368**[b], 462 (525)	527 (365)		694326	1
1b	332, 365, 400, **462** (525)	511 (365)		1452033	5
α-1c	328 (380) **365**, 435 (525) **537**, 584~ (640)	**400**, 488~, 533 (320) 495, **528** (420) **562**, 584~ (500)		1452034	8
β-1c	331~, **370**, 426 (525)	522 (365)		1574996	2
α-1d	318 (380) 331~, **370**, 427 (525)	378, **511** (320) 511 (365)		1452031	8
β-1d	275, 307~, **372**, 426 (525)	471 (365)		1574998	2
1e	318 (380) 334~, 368, 446 (525)	380, 414~, 508 (320) 511 (365)		1581463	9
1f	318 (380) **320**, 365~ (525)	**380**, 514 (320) 528 (365)		1580717	9
2a	322~, **373**, 426 (580)	553 (365)		1575039	4
2b	330~, **370**, 418 (525)	470 (365)		1575056	6
α-2c	322~, **369**, 452 (525) 320~, **369**, 450, 480~ (550)	505 (365) 554 (490)		1575015	7
β-2c	319 (380) 325~, **368**, 465 (525) 325~, 368, **476**, 524 (580)	379, **509** (320) 509 (365) 543 (525)		1575014	4
2d	320~, **369**, 455 (525)	521 (365)		1575020	3

Table 2 *(Contd.)*
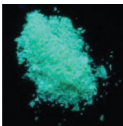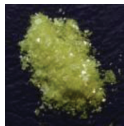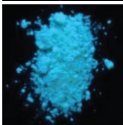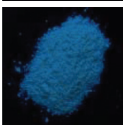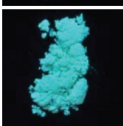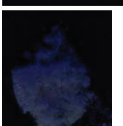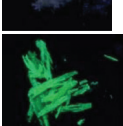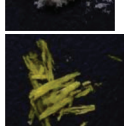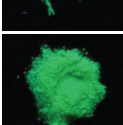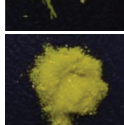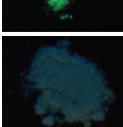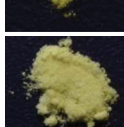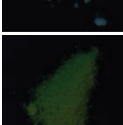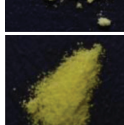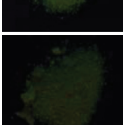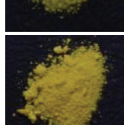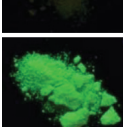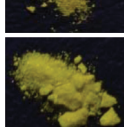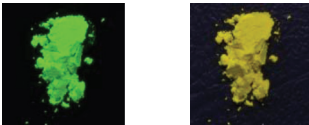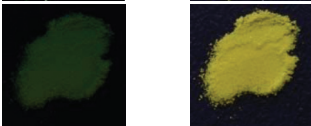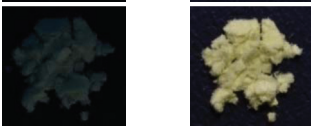
ATCN	λ_{max}^{ex} (λ^{reg}), nm	λ_{max}^{em} (λ^{ex}), nm	Visual appearance of the compounds under UV/visible light		CCDC	Structure type
2e	331~, **370**, 435 (525)	496 (365)			1575001	3
2f	334~, **372**, 424 (525)	485 (365)			1575038	4
3a	318 (380) 328, **368**, 413 (480) 325~, 365, **437**, 525 (580)	379, **482** (320) 488 (365) 591 (525)			1575023	2
3b	328~, **372**, 422 (525)	480 (365)			1575055	4
3c	326~, **370**, 423 (525)	496 (365)			1575016	2
α-3d	319 (380) 323~, 370, **418** (460) 325~, 368, **434**, 469~ (525)	375, **460** (320) 460 (365) 513 (450)			1575088	2
β-3d	276, 309~, **370**, 444 (525)	506 (365)			1575000	3
3e	328~, **370**, 450 (525)	504 (365)			1575021	3
3f	319 (380) 324~, **371**, 425 (525)	378, **484** (320) 484 (365)			No X-ray data	
4a	319 (380) 333~, **371**, 428 (525)	377, **513** (320) 513 (365)			1575024	1
4b	318 (380) 332, 370, 427, 485~ (525)	380, 476 (320) 476 (365)			1575057	6
4c	334~, **373**, 459 (525)	517 (365)			1575040	7

Table 2 *(Contd.)*

ATCN	λ_{max}^{ex} (λ^{reg}), nm	λ_{max}^{em} (λ^{ex}), nm	Visual appearance of the compounds under UV/visible light		CCDC	Structure type
4d	276, 307~, **369**, 465 (525)	527 (365)			1575041	3
4e	332~, **370**, 440 (525)	510 (365)			1575022	1
4f	318 (380) 327, **371**, 426 (525)	**379**, **486** (320) 489 (365)			1575037	10

[a] Shoulder ~. [b] Principal maximum in bold.

the solid state, **2f** possesses visible fluorescence at 450–600 nm (like most of the investigated tetracyanopropenide salts, see Table 2 and Fig. 9–32 in the ESI†), and **1f** possesses no visible fluorescence.

We then examined the fluorescence properties of cesium salt powders in the series **1f**, **4f**, **3f**, and **2f**. We have estimated that there is a fluorescence intensity increase in this row: **4f**, **3f**, and **2f** have absolute fluorescence quantum yields φ_{abs} equal to 0.6%, 1.9% and 16.7%, respectively; consequently, their fluorescence lifetimes τ are 7.4 ns, 4.5 ns, and 3.7 ns (**1f** fluorescence in the solid state is very weak). There are two emission optical centers (OC) in the **1f** fluorescence spectra: OC1 (λ_{max}^{em} = 380 nm, Fig. 26(c)) and OC2 (λ_{max}^{em} = 514 nm, Fig. 26(b)), and the OC1 band is more intense. The **1f** excitation spectra also consist of two bands – an intense band at 319 nm (OC1) and another band at 365 nm with low intensity (OC2), which can be seen only as a shoulder (see Fig. 14 in the ESI†). The OC1 and OC2 bands in the **4f** emission and exci-

tation spectra are almost of the same intensity (Fig. 27). The OC2 bands in the **3f** emission and excitation spectra are about ten times more intense as compared to the OC1 bands (Fig. 28). There is only an OC2 emission band in the **2f** spectra (λ_{max}^{em} = 485 nm), and the OC1 band in its excitation spectra can be seen only as a shoulder (Fig. 25(b)).

The fluorescence properties of the ATCN α and β polymorph modification are also different. We found out that the fluorescence of **β-1c**, **β-1d**, and **β-3d** is more intense than that of **α-1c**, **α-1d**, and **α-3d**. As we can see in Fig. 29, there are two OC bands in the **α-1d** emission and excitation spectra: OC1 (λ_{max}^{em} = 380 nm, λ_{max}^{ex} = 318 nm) and OC2 (λ_{max}^{em} = 511 nm, λ_{max}^{ex} = 435 nm). Moreover, only OC2 is responsible for the **β-1d** fluorescence (λ_{max}^{em} = 471 nm, λ_{max}^{ex} = 426 nm). For the **α-2c** and **β-2c** species, several OC bands are observed (see Table 2), and both these polymorphs show a weak fluorescence.

Fig. 27 Solid state **4f** emission and excitation spectra; excitation wavelength is 320 nm (green curve) and 365 nm (blue curve), registration wavelength is 380 nm (black curve) and 525 nm (red curve).
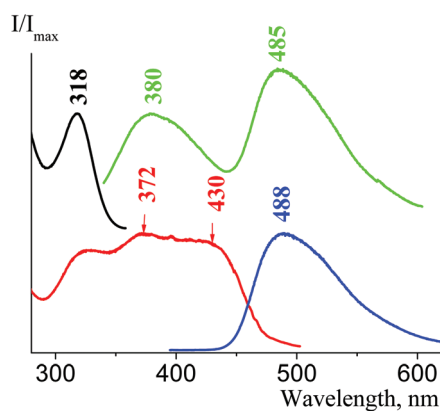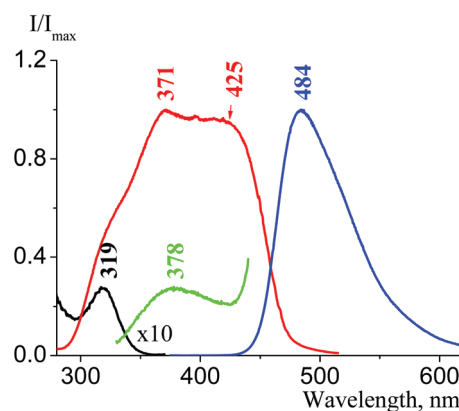

Fig. 28 Solid state **3f** emission and excitation spectra; excitation wavelength is 320 nm (green curve) and 365 nm (blue curve), and registration wavelength is 380 nm (black curve) and 525 nm (red curve). Black and green curves intensity are ten times multiplied.
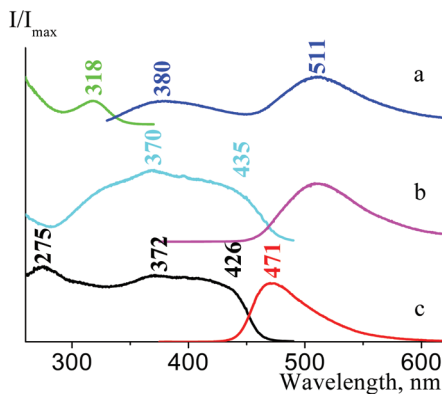
Fig. 29 Solid state α-**1d** (a and b) and β-**1d** (c) emission and excitation spectra; excitation wavelength is 320 nm (blue curve) and 365 nm (magenta and red curves), and registration wavelength is 380 nm (green curve) and 500 nm (cyan and black curves).
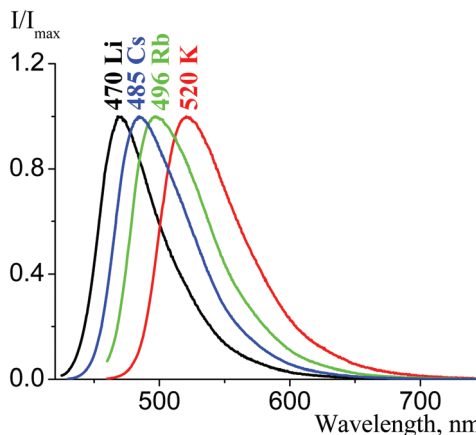

Fig. 30 Solid state emission spectra of **2b** (black curve, λ^{ex} = 450 nm), **2f** (blue curve, λ^{ex} = 420 nm), **2e** (green curve, λ^{ex} = 425 nm), and **2d** (red curve, λ^{ex} = 425 nm).

Comparison and discussion

The revealed fluorescence property differences of tetracyanopropenide salts in the solid state (or visible fluorescence origin) can be explained by a comparison of the obtained electron spectra and the results of the X-ray experiment for the same compounds. There are two types of interactions in the ATCN crystals: anion–anion (between different tetracyanoallyl fragments) and anion–cation (between CN-groups of tetracyanoallyl fragments and ammonia or alkali metal cation). Tetracyanoallyl fragments in the **1f** cesium salt crystal are not parallel, and the distances between their CN-groups are about 3.52–6.37 Å. In the **4f** crystals, these fragments are parallel, but shifted to each other, and the distances between them are a bit shorter and equal to 4.05–4.41 Å. In the **2f** crystals, the tetracyanoallyl fragments are parallel, turned to each other for about 90°; thus, the examined distances are shorter and equal to about 3.54–3.79 Å. For rubidium salts, these distances are about 3.49–5.47 Å for **1e**, 3.50–4.57 Å for **4e**, 3.55–4.54 Å for **3e**, and 3.45–3.61 Å for **2e**. In the case of **2f** and **2e** crystals, direct short contacts between tetracyanoallyl fragments of different ligands are detected. Anion–cation interactions for cesium and rubidium salts don't differ significantly. For cesium salts, each tetracyanoallyl fragment is coordinated with four (**1f**) or five (**4f** and **2f**) cesium cations. This type of cesium coordination can lead to distortion of tetracyanoallyl fragments: their torsion angles are equal: 10.8° for **1f**, 3.5° for **4f**, and 6.9° for **2f**. For rubidium salts, these values are similar.

The lack of visible fluorescence in ATCN dilute solutions and its origin in the solid state led us speculate that the fluorescence of powders was due to the intermolecular interactions, which didn't exist in solution. We suppose that the origin of the visible fluorescence is mainly due to the anion–anion interactions between tetracyanoallyl fragments at their parallel location at the distances of 3.5–4.0 Å (for different types of anion–anion interactions in the crystals see literature[20]). In this case, the fluorescence properties of tetracyanopropenide salts are determined by one OC of emission, and

these samples possess more intense fluorescence as compared to those that have several OCs. Further research is required to estimate the observed OC nature. It should be noted that the samples **1e** and **1f**, which show a weak fluorescence and have more intense OC1 emission bands than OC2 bands, belong to the same 9th structure type.

A characteristic feature of the tetracyanopropenide fluorescence spectra is that their emission maxima values correlate with distances between parallel tetracyanoallyl fragments. When these distances decrease in the series **2b**, **2f**, **2e**, and **2d** from 4.2 to 3.4 Å, fluorescence bands shift bathochromically by about 50 nm (Fig. 30). These results correspond to the analogous effect, which has been reported for tetracyanopirrolates.[21]

H-bond is another factor that influences the fluorescence properties of tetracyanopropenides in the solid state. H-bond existence between cation and anion (for **2a**) or between anion and molecules of solvated water (for **2c**) leads to emission band broadening (for about 2500 cm^{-1}, *i.e.* almost twice) and long-wavelength shift (Fig. 31). A more detailed study of
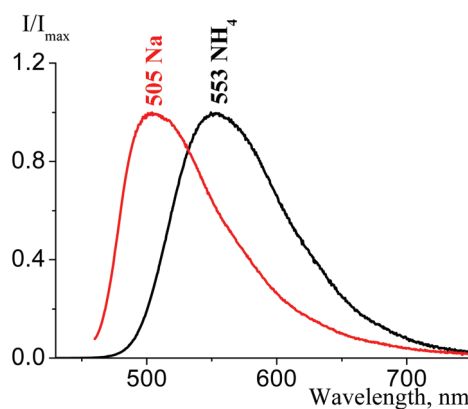

Fig. 31 Solid state emission spectra of **2a** (black curve, λ^{ex} = 420 nm) and α-**2c** (red curve, λ^{ex} = 450 nm).

H-bond influence on the emission spectra of tetracyanopropenides is required.

Conclusions

In conclusion, we have synthesized 24 ammonia and alkali metal ATCN salts, most of which have not been described previously. The crystal structures of 23 of them are reported. Some ATCN were obtained as two crystalline polymorphs. Moreover, ten structure types of these salts are described, three of which are predominant. In the solid state, most ATCN exhibit blue, green or yellow-green photoluminescence with nanosecond lifetimes. ATCN absorbance and fluorescence spectra in a dilute solution are almost the same. It is shown that ATCN fluorescence in the solid state is mainly originated due to intermolecular anion–anion interactions between different tetracyanoallyl fragments of ligands. Fluorescence band location and shape are mostly determined by distances between tetracyanoallyl fragments, their orientation to each other, and by the presence of H-bonds. ATCN might be used as bridging ligands for the construction of various 1D, 2D, and 3D coordination polymeric frameworks and potentially functional materials.

Conflicts of interest

There are no conflicts to declare.

Acknowledgements

Notes and references

1 (a) Z. Setifi, A. Valkonen, M. A. Fernandes, S. Nummelin, H. Boughzala, F. Setifi and C. Glidewell, *Acta Crystallogr., Sect. E: Struct. Rep. Online*, 2015, **71**, 509–515; (b) Z. Setifi, K. V. Domasevitch, F. Setifi, P. Mach, S. W. Ng, V. Petříček and M. Dušek, *Acta Crystallogr., Sect. C: Cryst. Struct. Commun.*, 2013, **69**(Pt 11), 1351–1356; (c) F. Setifi, D. K. Geiger, I. Abdul Razak and Z. Setifi, *Acta Crystallogr., Sect. C: Struct. Chem.*, 2015, **71**(Pt 8), 658–663; (d) Z. Setifi, F. Setifi, H. Boughzala, A. Beghidja and C. Glidewell, *Acta Crystallogr., Sect. C: Struct. Chem.*, 2014, **70**(Pt 5), 465–469; (e) Z. Setifi, F. Lehchili, F. Setifi, A. Beghidja, S. W. Ng and C. Glidewell, *Acta Crystallogr., Sect. C: Struct. Chem.*, 2014, **70**(Pt 3), 338–341; (f) B. Gaamoune, Z. Setifi, A. Beghidja, M. El-Ghozzi, F. Setifi and D. Avignant, *Acta Crystallogr., Sect. E: Struct. Rep. Online*, 2010, **66**(Pt 8), m1044–m1045.

2 (a) Z. Setifi, F. Setifi, L. El Ammari, M. El-Ghozzi, J. Sopková-de Oliveira Santos, H. Merazig and C. Glidewell, *Acta Crystallogr., Sect. C: Struct. Chem.*, 2014, **70**(Pt 1), 19–22; (b) Z. Setifi, B. Gaamoune, H. Stoeckli-Evans, D. A. Rouag and F. Setifi, *Acta Crystallogr., Sect. C: Cryst. Struct. Commun.*, 2010, **66**(Pt 10), m286–m289; (c) T. Franck and S. P. Jean, *Polyhedron*, 2003, **22**, 1837–1843; (d) E. I. Klimova, M. M. Garcia, M. Flores-Alamo, A. V. Churakov, S. Cortez Maya and I. P. Beletskaya, *Polyhedron*, 2014, **68**, 272–278; (e) S. Duclos, F. Conan, S. Triki, Y. Le Mest, M. Liu-Gonzalez and J. Sala-Pala, *Polyhedron*, 1999, **18**, 1935–1939; (f) F. Thetiot, S. Triki, J. Sala-Pala and S. Golhen, *Inorg. Chim. Acta*, 2005, **358**, 3277–3282; (g) Y. Funasako, K.-I. Abe and T. Mochida, *Thermochim. Acta*, 2012, **532**, 78–82; (h) Asrial, F. Olbrich, M. Spoida, A. Fischer and F. T. Edelmann, *Anorg. Allg. Chem.*, 2011, **637**, 190–194.

3 (a) S. Shuichi, K. Akihiko, Y. Hideki and S. Gunzi, *Mol. Cryst. Liq. Cryst.*, 2002, **376**, 207–212; (b) S. Shuichi, T. Chiyoko, Y. Hideki and S. Gunzi, *J. Mater. Chem.*, 2001, **11**, 2293–2302; (c) Y. Hideki, T. Chiyoko, S. Shuichi, S. Gunzi, K. Masami and S. Ken-Ichi, *Mol. Cryst. Liq. Cryst.*, 1996, **284**, 379–390; (d) S. Benmansour, M. Marchivie, S. Triki and C. J. Gómez-García, *Crystals*, 2012, **2**, 306–326; (e) S. Shuichi, N. Matsukawa, Y. Hideki and S. Gunzi, *Synth. Met.*, 2003, **133**, 455–457; (f) S. Shuichi, Y. Hideki and S. Gunzi, *Synth. Met.*, 2003, **135**, 631–632.

4 G. Dupouy, S. Triki, M. Marchivie, N. Cosquer, C.-J. Gomez-Garcia, S. Pillet, E.-E. Bendeif, C. Lecomte, S. Asthana and J.-F. Letard, *Inorg. Chem.*, 2010, **49**, 9358–9368.

5 (a) J. A. Schlueter and U. Geiser, *Acta Crystallogr., Sect. C: Cryst. Struct. Commun.*, 2003, **59**(Pt 4), M146–M148; (b) B. Samia, T. Smail and J. G.-G. Carlos, *Magnetochemistry*, 2016, **2**, 1–15; (c) A. Abderezak, S. Fatima, G. K. Konstantin, G. Christopher, S. Zouaoui, S. Graham and R. Jan, *Polyhedron*, 2015, **87**, 307–310; (d) Y. Consuelo, B. Abdeslem, M. Nadia, A. Donatella, S. Fatima, T. Smail, L. Francesc and J. Miguel, *Polyhedron*, 2009, **28**, 1287–1294; (e) S. Triki, J. Sala-Pala, M. Decoster, P. Molinie and L. Toupet, *Angew. Chem., Int. Ed.*, 1999, **38**, 113–115; (f) S. Triki, F. Thetiot, F. Vandevelde, J. Sala-Pala and C.-J. Gomez-Garcia, *Inorg. Chem.*, 2005, **44**, 4086–4093; (g) E. Lefebvre, F. Conan, N. Cosquer, J.-M. Kerbaol, M. Marchivie, J. Sala-Pala, M. Kubicki, E. Vigier and C.-J. Gomez-Garcia, *New J. Chem.*, 2006, **30**, 1197–1206; (h) M. L. Yates, A. M. Ari, J. L. Manson, B. A. Kalm, B. B. Burkhart and J. S. Miller, *Inorg. Chem.*, 1998, **37**, 840–841.

6 (a) G. Dupouy, M. Marchivie, S. Triki, J. Sala-Pala, C. J. Gomez-Garcia, S. Pillet, C. Lecomte and J. F. Letard, *Chem. Commun.*, 2009, 3404–3406; (b) G. Dupouy, S. Triki, M. Marchivie, N. Cosquer, C. J. Gomez-García, S. Pillet, E.-E. Bendeif, C. Lecomte, S. Asthana and J.-F. Letard, *Inorg. Chem.*, 2010, **49**, 9358–9368.

7 (a) D. Gaelle, M. Mathieu, T. Smail, S.-P. Jean, S. Jean-Yves, J. G.-G. Carlos and G. Philippe, *Inorg. Chem.*, 2008, **47**,

8921–8931; (b) B. Samia, A. Chahlae, S. Fatima, T. Smaïl, M. Mathieu and J. G.-G. Carlos, *Coord. Chem. Rev.*, 2010, **254**, 1468–1478; (c) G. Dupouy, M. Marchivie, S. Triki, J. Sala-Pala, C. J. Gomez-García, S. Pillet, C. Lecomte and J.-F. Letard, *Chem. Commun.*, 2009, 3404–3406.

8 Y. Yukihiro, K. Masatoshi and S. Gunzi, *J. Phys. Chem. B*, 2009, **113**(26), 8960–8966.

9 S. Ilya, W. M. Timothy and W. James, *J. Phys. Chem. B*, 2013, **117**(23), 7084–7094.

10 (a) H. Gao, Z. Zeng, B. Twamley and J. M. Shreeve, *Chem. – Eur. J.*, 2008, **14**, 1282–1290; (b) Z. Dongmei, L. Jizhen, B. Fuqiang, Y. Yahui, G. Xiaoni, Z. Weiqiang, Z. Guofang and G. Ziwei, *Z. Naturforsch., B: Chem. Sci.*, 2015, **70**, 317–326.

11 (a) X. Liu, J. Li, F. Bi, W. Zhang, G. Zhang and Z. Gao, *Eur. J. Inorg. Chem.*, 2015, 1496–1504; (b) S. Ersha, L. Dongdong, L. Jizhen, Z. Guofang, Z. Weiqiang and G. Ziwei, *Z. Anorg. Allg. Chem.*, 2016, **642**, 871–881.

12 L. Yan, T. Ling-Zhi and Z. Shu-Zhong, *Inorg. Chem. Commun.*, 2017, **75**, 49–53.

13 B.-M. Anna, M. N. Gene, Ż. Grażyna, Z. Aldona, P. Marcin, T. Tomasz, D. Maciej, K. Michał, J. Piotr, N. Leszek, Z. Janusz, M. Marek and W. Władysław, *Sci. Rep.*, 2017, **7**, AN: 40036.

14 A. Samir, S. Carla and K. George, *J. Therm. Anal. Calorim.*, 2015, **119**(2), 1171–1182.

15 (a) S. V. Karpov, A. A. Grigor'ev, Y. S. Kayukov, I. V. Karpova, O. E. Nasakin and V. A. Tafeenko, *J. Org. Chem.*, 2016, **81**, 6402–6408; (b) S. V. Karpov, Y. S. Kaukov, A. A. Grigor'ev, O. E. Nasakin, O. V. Kaukova and V. A. Tafeenko, *Org. Biomol. Chem.*, 2016, **14**, 3758–3764.

16 A. Maciejewski and R. P. Steer, *J. Photochem.*, 1986, **1**, 59–69.

17 C. Würth, M. Grabolle, J. Pauli, M. Spieles and U. Resch-Genger, *Nat. Protoc.*, 2013, **8**, 1535–1550.

18 F. Neese, The ORCA program system, *Wiley Interdiscip. Rev.: Comput. Mol. Sci.*, 2012, **2**(1), 73–78.

19 *Luminescent analysis*, ed. G. I. Romanovskaya (in Russian), Moscow, Nauka, 2015.

20 Y. V. Nelyubina, M. Y. Antipin and K. A. Lyssenko, *Russ. Chem. Rev.*, 2010, **79**, 167–188.

21 V. A. Tafeenko, S. I. Gurskiy, A. N. Baranov, T. V. Kaisarova and L. A. Aslanov, *Acta Crystallogr., Sect. C: Cryst. Struct. Commun.*, 2009, **65**, m52–m55.